Control Engineering Practice 172 (2026) 106888

Contents lists available at ScienceDirect

Control Engineering Practice

journal homepage: www.elsevier.com/locate/conengprac

Predictive control of wastewater treatment plants as energy-autonomous water resource recovery facilities

Otacílio B. L. Neto [a,*], Michela Mulas [b], Iiro Harjunkoski [a], Francesco Corona [a]

[a] School of Chemical Engineering, Aalto University, Finland
[b] Department of Teleinformatics Engineering, Federal University of Ceará, Brazil

ARTICLE INFO

Keywords:
Wastewater treatment plant
Water resource recovery
Process control and automation
Model predictive control
Moving horizon estimation

ABSTRACT

This work proposes an automatic control solution for the operation of conventional wastewater treatment plants (WWTPs) as energy-autonomous water resource recovery facilities. We first conceptualize a classification of the quality of treated water for three resource recovery applications (environmental, industrial, and agricultural water reuse). We then present an output-feedback model predictive controller (Output MPC) that operates a plant to produce water of a specific quality class, while also producing sufficient biogas to ensure nonpositive energy costs. Using well-established simulation models, we analyze the controller performance on the long-term operation of a biological WWTP subjected to typical influent loads and periodically changing quality targets. Our experiments show that conventional WWTPs are flexible enough to transition from pollution abatement to resource recovery. The plant is also shown to have an energy-positive operating regime, that is, it can recover more energy than needed for its operation. Under closed-loop operation, the WWTP achieves the nutrient recovery targets while producing 83 GWh/year of surplus energy, with an average throughput of 2 385 kWh/day. The results provide a proof-of-concept for the energy-autonomous operation of existing wastewater treatment infrastructure with control strategies that are general enough to accommodate different resource recovery tasks.

1. Introduction

A paradigm shift in the management of water resources is taking place: Wastewater, traditionally seen as a pollutant, is now recognized as a sustainable source of clean water, energy, and nutrients (Guest et al., 2009; Kundu et al., 2022; Ricart & Rico, 2019; Verstraete & Vlaeminck, 2011; United Nations, 2017). The potential to commodify these resources, together with increasing water demands and environmental concerns, is driving the wastewater sector to rethink wastewater treatment plants (WWTPs) as *water resource recovery facilities* (WRRFs) (Kehrein et al., 2020; Sarpong & Gude, 2020). Recovering nutrients directly to effluent streams, thus producing reused water of tailored quality, has become a particularly attractive process goal: Aside from promoting a circular economy and zero-waste principles, such a practice alleviates water stress by conserving freshwater resources for the provision of potable water. Moreover, a balanced water-energy nexus can be achieved by harvesting the excess sludge from this process for heat and electrical energy. A technology able to produce reused water of tailored quality while still having net-zero (or even net-negative) energy balance costs thus contributes an essential step in the transition from wastewater treatment to water resource recovery.

Current research efforts focus on redesigning and upgrading treatment plants with new dedicated process units. Novel nutrient recovery processes include crystallizers for struvite precipitation (Peng et al., 2018), membrane-based processes for concentrating nitrogen via forward osmosis and ultrafiltration (Wu, 2019; Xie et al., 2016), and bioreactors promoting micro-algae cultivation (Li et al., 2019; Valverde-Pérez et al., 2015). Energy recovery is commonly proposed by integrating combined heat and power (CHP) systems to treatment plants and rearranging their units to maximize the production of biofuels from waste (Sarpong & Gude, 2020; Solon et al., 2019; Wan et al., 2016). In the aforementioned processes, source-separating systems for splitting domestic wastewater into urine, greywater, and blackwater are often a relevant pre-treatment step. While promising, the costs of building and operating such technologies (Chen & Wang, 2009; Faragò et al., 2021) have undeniably slowed their implementation. In contrast, little has been investigated on the potential for repurposing the already in-place infrastructure by reprogramming its operation for water resource recovery goals. In this direction, biological treatment of wastewater (Henze et al., 2008) offers a promising platform: Such a treatment infrastructure is common to most urban centers, has a recognized potential for energy recovery through the production of biogas, and is centred on controlling the

* Corresponding author.
E-mail address: otacilio.neto@aalto.fi (O. B. L. Neto).

https://doi.org/10.1016/j.conengprac.2026.106888
Received 18 August 2025; Received in revised form 4 February 2026; Accepted 26 February 2026
Available online 5 March 2026

nitrogen and phosphorus content of wastewater–two major nutrients lost by conventional treatment. Finally, these bioprocesses are increasingly instrumented and digitalized, thus facilitating the design and deployment of new operation policies.

Biological WWTPs are large-scale dynamical systems of notorious complexity. Their real-time operation thus requires control solutions capable of automatically driving actuators using data from *in situ* sensors. Traditionally, this was achieved by low-level regulators that controlled key process variables to match operational targets set during process design (Åmand et al., 2013; Olsson et al., 2013). Model predictive control (MPC, Rawlings et al., 2020) soon emerged as a promising approach for optimizing the performance of biological WWTPs performing pollution abatement. For the specific tasks of dissolved oxygen and nitrogen control, setpoint tracking MPC outperforms low-level regulators (Foscoliano et al., 2016; Han et al., 2012; Holenda et al., 2008; Mulas et al., 2015; O'brien et al., 2011; Santín et al., 2016). The existing solutions cover different types of biological WWTPs, using either first-principles or black-box models to represent their dynamics, and are mostly based on classical MPC algorithms. In the same direction, Shen et al. (2008) proposed a MPC for enforcing regulation-type limits on the plant's effluent quality. For the higher-level task of enforcing effluent quality limits while simultaneously minimizing the plant's energy costs, different MPC strategies were proposed: these include multi-level (Brdys et al., 2008; Francisco et al., 2015; Vega et al., 2014), multi-objective (Han et al., 2014), and economic (Stentoft et al., 2020; Zeng & Liu, 2015; Zhang et al., 2019) MPC formulations. In general, such controllers either directly optimize the effluent quality and operating cost indices achieved by the closed-loop system, or explicitly constrain the effluent concentration of pollutants. The technological scope has also been extended to include model-based state estimation, for both monitoring and control purposes (Busch et al., 2013; Yin et al., 2018; Yin & Liu, 2019). Finally, the latest developments consider learning-based methods, such as Koopman operators (Han et al., 2024) and neural networks (Bernardelli et al., 2020; Han et al., 2022; Wang et al., 2023), to improve existing MPC strategies and produce more accurate (and numerically convenient) process models.

The research on the predictive control of biological WWTPs, while active, has remained limited to *ad-hoc* designs tailored to nutrient removal. Despite the aforementioned large pool of control solutions, there are still no results on operating conventional WWTPs for resource recovery. In previous work, we addressed this research gap by proposing a general control framework for biological WWTPs (Neto et al., 2024). The framework is centred on an output-feedback MPC for reference-tracking, with the references designed to reflect higher-level environmental and/or economic objectives. In this work, we specialize this control framework and investigate its performance in operating full-scale biological WWTPs as self-sufficient WRRFs. Specifically, we

(i) classify the quality of treated water in terms of its biochemical profile, based on three target applications (environmental, industrial, and agricultural reuse);
(ii) design an output-feedback MPC to operate a conventional WWTP to produce water of different quality classes, while enforcing non-positive energy costs;
(iii) demonstrate this controller on the long-term operation of a WWTP subjected to typical influent loads.

The predictive controller is a digital solution whose functioning depends on a dynamic model of the process and its operation relies on the exchange of data with the plant's actuators (the control actions) and sensors (the measurements). We design its main components such that it achieves energy-autonomous resource recovery by tracking a desired water quality grade, while still enforcing that the operation has nonpositive energy costs. The controller is configured under the assumption that the targeted water quality changes periodically to supply alternating clients with reclaimed water. While this setup is specific, the controller architecture is general enough to accommodate a wider range of

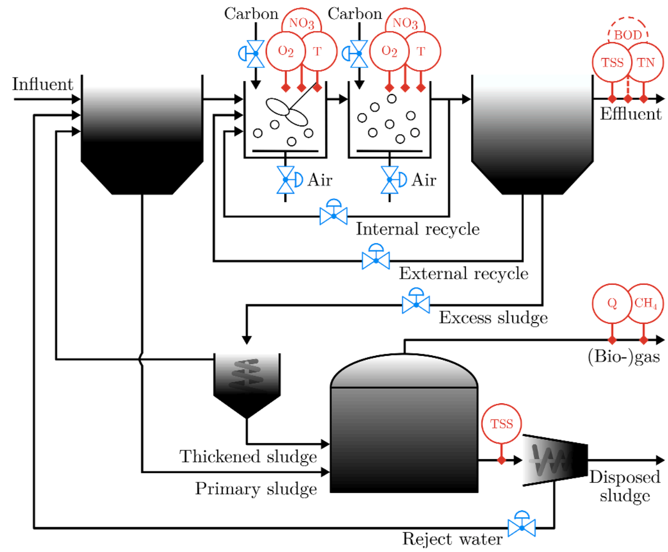

Fig. 1. Process layout of a WWTP. The solid balloons refer to quantities measurable through online sensors, while the dashed balloons refer to quantities measurable only through laboratory analysis.

treatment processes and resource recovery objectives. Our experiments are carried out at a simulation level and the results contribute a proof-of-concept on the flexibility of conventional wastewater treatment infrastructures.

The rest of the paper is organized as follows: Section 2 overviews biological WWTPs, provides a classification of reused water quality, and then presents the benchmark model used to represent and simulate real-world facilities. Section 3 overviews the output-feedback predictive controller, its individual components, and their specific configuration for the energy-autonomous operation of WWTPs as WRRFs. Section 4 presents and discusses the simulation results of operating a conventional WWTP using our predictive controller. Finally, Section 5 provides concluding remarks. For the model equations and additional technical details, we refer to the Supplementary Material.

2. The water resource recovery facility: Process layout, water quality classes, and simulation setup

We consider a conventional biological wastewater treatment plant (WWTP, Henze et al., 2008) comprised of two main processes:

- The activated sludge process, in the *water line*, based on nitrification-denitrification processes, in which microorganisms reduce ammonia present in the wastewater into nitrate, which is then further reduced into nitrogen gas and released into the atmosphere;
- The anaerobic digestion process, in the *sludge line*, in which organic material present in the excess sludge produced by the plant is converted into biogas, which is used as fuel for heat and energy generation.

In a typical process (Fig. 1), the water line comprises two reacting sections and a settling tank. Each reacting section may consist of several zones for the oxidation of organic matter. The settler clarifies the treated water from suspended solids and flocculated particles before it is further processed or disposed. The sludge line typically comprises a thickener unit, an anaerobic digester, and a dewatering unit. The thickener and dewatering units are solid-separation processes that reduce the volume of the sludge fed to and disposed from the digester, respectively.

In general, a WWTP can be understood as a process that converts influent wastewater into three main products: treated (or reclaimed) water, biogas, and disposed sludge. When no further processes exist downstream, any quality requirements must be applied directly to these effluents. The quality of the treated water is characterized by its concentrations of total suspended solids (TSS), organic matter (quantified as biochemical oxygen demand, BOD), and total nitrogen (TN, the sum of organic nitrogen, ammonia, and nitrates/nitrites). The quality of the biogas is characterized by its concentration of methane (CH_4). The quality of the disposed sludge is indirectly characterized by the concentrations of total suspended solids (TSS) in the outflow of the digester. During operation, these quantities are routinely monitored through instrumentation consisting of both analyzers and online sensors. Additional sensors (e.g., flow-rate, temperature, volume) are often deployed to further observe the operating conditions of the process.

Remark 1. The quality of the treated water can include additional metrics such as its concentrations of phosphorus and pathogens. As these are treated by external or tertiary processes, they are not considered in our study. Regardless, our control framework (Section 3) can still be configured to incorporate such processes in the plant's layout–provided that a model of their dynamics is available.

A modern treatment plant might employ different solutions from control engineering to automate its operation (Olsson et al., 2013). This is required to ensure effluents of consistent quality despite the variability of the influent. Many control strategies are built upon two conventional feedback loops:

- Nitrate nitrogen (NO_3-N) in the anoxic section is controlled by manipulating the internal recirculation;
- Dissolved oxygen (O_2) in the aerated section is controlled by manipulating the air flow-rate.

Using low-level regulators (Seborg et al., 2016), those measurable quantities are driven towards set-points provided manually by the plant's operators to achieve a specified effluent quality. In more advanced strategies, these set-points are instead determined by higher-level control systems to optimally achieve a given objective under operational constraints. To operate a WWTP as an energy-autonomous WRRF (that is, to produce reused water of tailored quality with net-zero energy costs), such advanced solutions become necessary.

In the following, we define control objectives for this class of treatment plants when operated for resource recovery. For the task of producing reused water with net-zero energy costs, we characterize three water quality classes based on environmental, industrial, and agricultural demands, and we present a quantitative metric of the energy being consumed (or generated) by the plant's operation. We conclude the section by describing the model and data used to simulate a WWTP for validating our proposed control system (Section 3) given these newly established targets.

2.1. Water quality classes and control objectives

The primary control objective of an energy-autonomous WRRF consists of targeting different qualities for its effluent water. Considering three major applications of reclaimed water (environmental, industrial, and agricultural reuse), the plant should be able to switch between producing:

Class A) water suitable for sustaining and/or augmenting natural water bodies;
Class B) water suitable for urban (e.g., toilet flushing) and industrial (e.g., cooling systems) activities;
Class C) water suitable for crop irrigation.

The classification is defined via upper limits on the effluent quality metrics (that is, concentrations of suspended solids, organic matter, and nitrogen), such that, would the treated water be used for the aforementioned purposes, no harmful side effects are expected. We consider the limits reported in Table 1, based on existing regulations and well-established standards (Alcalde-Sanz, 2017; EU, 2020; EPA, 2012; Shoushtarian & Negahban-Azar, 2020). In practice, solids and organic matter must always be kept at low levels to avoid bacterial growth and accumulation of inert matter. Conversely, being a nutrient, nitrogen has less stringent limits depending on the application: While not critical for industry, it is a valuable resource for agriculture. The limit on the nitrogen content of fertigation water (Class C) is then only meant to avoid issues related to the oversupply of nutrients (Albornoz, 2016).

Table 1
Water quality classes and their characterization in terms of the effluent concentrations of total suspended solids (TSS), biochemical oxygen demand (BOD), and total nitrogen (TN).

Water class	Biochemical profile		
	TSS	BOD	TN
A	≤ 30 g/m^3	≤ 10 g/m^3	≤ 15 g/m^3
B	≤ 30 g/m^3	≤ 15 g/m^3	≤ 30 g/m^3
C	≤ 30 g/m^3	≤ 20 g/m^3	≤ 45 g/m^3

The real-time operation of the WWTP to produce effluents of either quality requires an external (time-varying) demand for that specific water. In the absence of explicit clients, we instead assume the control objective to change periodically. Specifically, we assume that the plant alternates between producing water of Class A and Class B on a monthly basis. In this case, the plant compensates for an energy-intensive task (targeting Class A) with a less expensive operation (targeting Class B). Exceptionally, Class C is the targeted quality during cold seasons: This is to exploit the performance of the plant during winter, considering that nitrogen removal is especially difficult at low temperatures and that greenhouse farming would still create demands for irrigation water during this period.

Remark 2. The scenario used for this study is specific but not restrictive. Our control strategy is also valid when the quality targets are given in real-time by external clients.

The secondary control objective of an energy-autonomous WRRF consists of adjusting its biogas production to recover the energetic costs incurred by its operation. For this class of WWTPs, we quantify the net demand of electricity and heating using the energy cost index (ECI, in kWh/d),

$$\mathrm{ECI} = \mathrm{AE} + \mathrm{PE} + \mathrm{ME} - \eta_E \mathrm{MP} + \max(0, \mathrm{HE} - \eta_H \mathrm{MP}) \tag{1}$$

given the aeration (AE, kWh/d), pumping (PE, kWh/d), mixing (ME, kWh/d), and heating (HE, kWh/d) energy required for operation. Energy generated from effluent biogas is expressed as methane production (MP, in kg CH_4/d) converted to electricity (with efficiency $\eta_E > 0$) and heat (with efficiency $\eta_H > 0$). At any given time, these metrics are determined from the value of the process state and of the control actions requested to its actuators. A WWTP is then characterized as energy-autonomous when its ECI, averaged over a specified period, is nonpositive.

2.2. Model and simulation data

The Benchmark Simulation Model no. 2 (BSM2, Gernaey et al., 2014) is used in this work to represent a large-scale treatment plant. The BSM is the *de facto* platform for control design and simulation of biological treatment plants subject to typical municipal influents (Brdys et al., 2008; Busch et al., 2013; Foscoliano et al., 2016; Francisco et al., 2015; Han et al., 2022, 2014, 2012, 2024; Neto et al., 2024; Olsson et al., 2013; Santín et al., 2016; Shen et al., 2008; Stentoft et al., 2020; Vega et al., 2014; Wang et al., 2023; Yin et al., 2018; Yin & Liu, 2019; Zeng & Liu, 2015; Zhang et al., 2019). It consists of a description of a plant's layout, a model of its dynamics and measurement process, and influent data for its simulation.

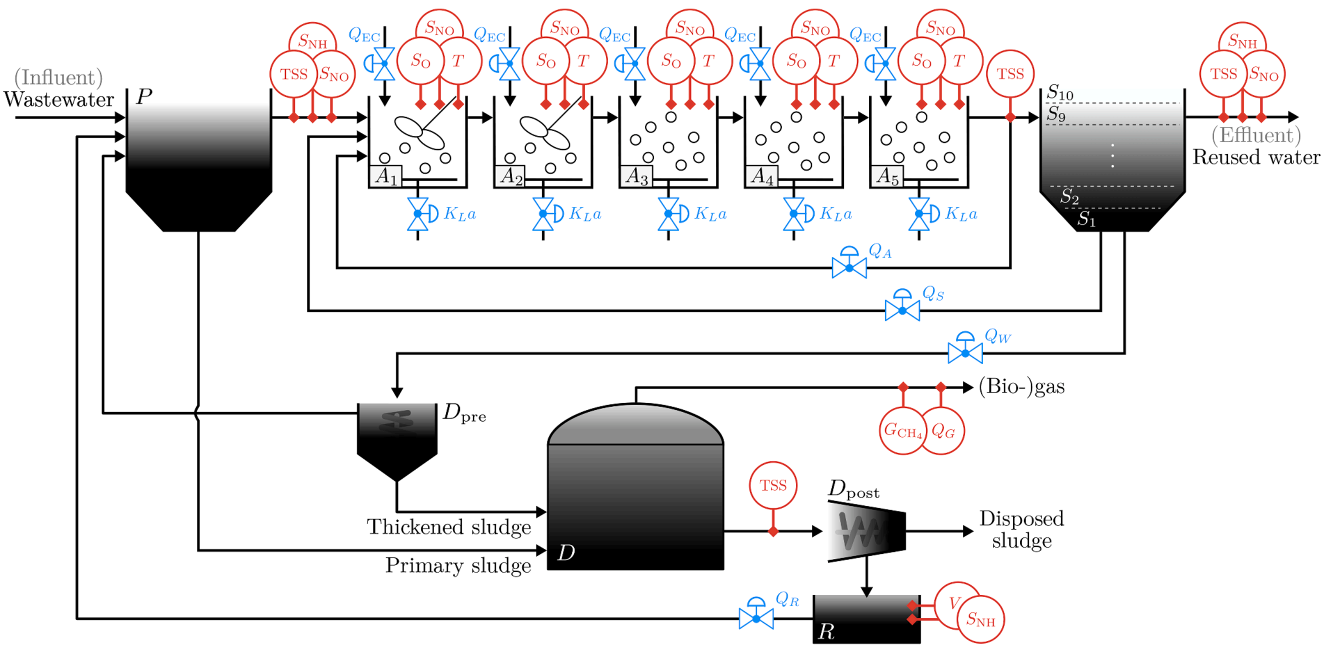

Fig. 2. Process actuation and instrumentation layout for the Benchmark Simulation Model no. 2 (BSM2).

The benchmark describes a conventional biological WWTP (Fig. 2) whose water line is comprised of

- a series of 5 bioreactors (denoted $A_1, \ldots, A_5$), with dynamics by the Activated Sludge Model no. 1 (Henze et al., 2000). For each rth reactor, the inflow of air ($K_La^{A_r}$) and carbon ($Q_{\mathrm{EC}}^{A_r}$) can be manipulated, and we monitor its temperature (T^{A_r}) and concentrations of dissolved oxygen ($S_{\mathrm{O}}^{A_r}$) and nitrate-plus-nitrite nitrogen ($S_{\mathrm{NO}}^{A_r}$). The outflow concentrations of total suspended solids from the water line (TSS^{A_5}) are also monitored;
- a non-reactive settler represented by 10 vertical layers ($S_1, \ldots, S_{10}$) with dynamics by Takács et al. (1991). From its topmost layer (S_{10}), the concentrations of suspended solids ($\mathrm{TSS}^{S_{10}}$), soluble ammonia ($S_{\mathrm{NH}}^{S_{10}}$), and nitrate-plus-nitrite nitrogen ($S_{\mathrm{NO}}^{S_{10}}$), are monitored. The chemical profile in S_{10} characterizes the effluent water quality;

and the sludge line is comprised of

- a thickener (D_{pre}) and a dewatering (D_{post}) unit, both described as ideal solid separation processes;
- an anaerobic digester (D), with dynamics by the Anaerobic Digestion Model no. 1 (Batstone et al., 2002). This unit is monitored through its effluent gas flow-rate (Q_{gas}^{D}) and methane composition ($G_{\mathrm{CH_4}}^{D}$), and through its outflow concentrations of suspended solids (TSS^{D});
- a non-reactive storage tank for reject water (R), with basic mass flow dynamics. Its liquid volume (V^R) and concentrations of ammonia (S_{NH}^{R}) are monitored.

The primary clarifier (P) has dynamics described by Otterpohl (1995). As in the settler, its overflow (P_{eff}, fed to the water line) is monitored by its concentrations of total suspended solids ($\mathrm{TSS}^{P_{\mathrm{eff}}}$), ammonia ($S_{\mathrm{NH}}^{P_{\mathrm{eff}}}$) and nitrate-plus-nitrite ($S_{\mathrm{NO}}^{P_{\mathrm{eff}}}$) nitrogen. Finally, water and sludge can be recirculated in the plant through the internal (Q_A), external (Q_S), excess sludge (Q_W) and reject water (Q_R) recycle flow-rates.

The benchmark WWTP consists of a process with a total of $N_u = 14$ actionable inputs and $N_y = 27$ measurable outputs. Under this layout, the BSM2 provides a unified dynamical model describing the plant in terms of $N_x = 225$ state variables (the chemical concentrations and temperature in all units), how they evolve in response to external inputs (the influent wastewater and control actions), and how they are emitted in the measurements. The model also describes how the state determines the instantaneous value of the $N_z = 4$ key performance indicators (KPIs): The effluent total suspended solids ($\mathrm{TSS}^{\mathrm{eff}}$), 5-days measured biochemical oxygen demand ($\mathrm{BOD}_5^{\mathrm{eff}}$), total nitrogen ($\mathrm{TN}^{\mathrm{eff}}$), and the plant's energy cost index (ECI). We refer to Table 2 for a summary of the input-output variables for this process. The complete description of the state-space model is provided in the Supplementary Material.

Table 2
Actionable inputs, measurable outputs, and KPIs, for the Benchmark Simulation Model no. 2 (BSM2).

	Description [Units]	Location
Input		
Q_A	Internal recycle flow-rate [$\mathrm{m^3/d}$]	–
Q_S	External recycle flow-rate [$\mathrm{m^3/d}$]	–
Q_W	Excess sludge flow-rate [$\mathrm{m^3/d}$]	–
Q_R	Reject water flow-rate [$\mathrm{m^3/d}$]	–
K_La	Oxygen transfer coefficient [1/d]	$A_{1\rightsquigarrow5}$
Q_{EC}	External carbon flow-rate [$\mathrm{m^3/d}$]	$A_{1\rightsquigarrow5}$
Output		
TSS	Total suspended solids [$\mathrm{g/m^3}$]	P_{eff}, A_5, S_{10}, D
S_{NH}	$\mathrm{NH_4^+ + NH_3}$ nitrogen [$\mathrm{g/m^3}$]	P_{eff}, S_{10}, R
S_{NO}	$\mathrm{NO_3^- + NO_2^-}$ nitrogen [$\mathrm{g/m^3}$]	P_{eff}, $A_{1\rightsquigarrow5}$, S_{10}
S_{O}	Dissolved oxygen [$\mathrm{g/m^3}$]	$A_{1\rightsquigarrow5}$
T	Temperature [°C]	$A_{1\rightsquigarrow5}$
$G_{\mathrm{CH_4}}$	Methane [$\mathrm{kg/m^3}$]	D
Q_G	Gas flow-rate [$\mathrm{m^3/d}$]	D
V	Volume [$\mathrm{m^3}$]	R
KPI		
$\mathrm{TSS}^{\mathrm{eff}}$	Effluent total suspended solids [$\mathrm{g/m^3}$]	–
$\mathrm{BOD}_5^{\mathrm{eff}}$	Effluent 5-days measured BOD [$\mathrm{g/m^3}$]	–
$\mathrm{TN}^{\mathrm{eff}}$	Effluent total nitrogen [$\mathrm{g/m^3}$]	–
ECI	Energy cost index [kWh/d]	–

The actuation and instrumentation setup in this plant extends the typical WWTP layout (Fig. 1). Here, all bioreactors are equally equipped and both the primary and secondary effluents are monitored. This setup assumes that all the control handles (described by the

BSM2) are actionable and can be used for designing control policies (Gernaey et al., 2014). Under this assumption, we have the flexibility to dynamically adjust the anoxic/aerated volumes in the water line beyond the canonical schemes tailored for nitrogen removal–thus having a finer control of the nitrification-denitrification process. Specifically, it allows for the automatic adjustment of air ($K_L a$) or external carbon (Q_{EC}) flow-rates based on whether the current resource recovery objective requires the plant to perform nitrification or carbon-assisted denitrification. Monitoring primary effluent gives direct information on the wastewater entering the water line, aiding controllers in this planning. Despite extensive, such a layout is still realistic and comprised of commercially available sensors and actuators (Olsson et al., 2005). A formal analysis of the most cost-efficient control layout is beyond the scope of this paper.

Characterization of the influent wastewater

The BSM2 is accompanied by wastewater data (Fig. 3) describing the influent flow-rate, its temperature, and its biochemical profile in terms of 13 chemical concentrations. The data is based on observations from real plants and adapted to represent a 80 000 population-equivalent influent load, as described in Gernaey et al. (2011). It consists of $N_w = 1 + 1 + 13 = 15$ time series sampled every 15 min (≈ 0.01 days) over a period of 609 days. The sampling period is sufficient to capture the dynamics of the whole treatment process (Gernaey et al., 2014, §9.5). The influent is always of the municipal kind and non-actionable: it is treated as an unmeasured disturbance. Exceptionally, as is common practice, the influent flow-rate and its temperature are measured in real-time (Olsson et al., 2005). We remark that this partial monitoring of the influent benefits the design of state estimators, as it reduces the dimensionality of the estimation problem (Rawlings et al., 2020).

We focus on controlling the WWTP when subjected to the first 365 days of this influent scenario. In Fig. 3, we summarize the influent wastewater during this period in terms of its flow-rate (Q_{in}), temperature (T^{in}), concentrations of total suspended solids ($\mathrm{TSS}^{\mathrm{in}}$), biochemical oxygen demand ($\mathrm{BOD}_5^{\mathrm{in}}$) and total nitrogen ($\mathrm{TN}^{\mathrm{in}}$). For the latter, we highlight that most influent nitrogen occurs in the form of either organic or ammonium nitrogen. In addition to the seasonality (as per the temperature changes), we remark on the storm and rain events occurring over this scenario: They are characterized by sudden increases in the influent flow-rate and simultaneous dilution of its solids and nitrogen content. Since deviating noticeably from the average conditions, these are considered extreme events from the perspective of designing control strategies.

3. The predictive controller: Overview and specific setup for resource recovery tasks

Output model predictive control (Output MPC, Neto et al., 2024; Rawlings et al., 2020) is a systematic approach to design and execute controllers to operate physical systems according to practical objectives while subject to operational and technological restrictions. For operating WWTPs as energy-autonomous WRRFs, our Output MPC (Fig. 4) comprises three main computational units: an operating point optimizer (OPO); a model predictive controller (MPC); and a moving horizon estimator (MHE). Formally, these units compute solutions to optimization problems based on a predictive model of the system's response to external inputs. The OPO prepares an operating point that, if enforced, leads to some desired values for the process' KPIs (the water quality metrics and energy cost index). Using this operating point as a reference, the MHE and MPC respectively determine the process' current state and the sequence of control actions that would stabilize it around the desired set-point.

The Output MPC operates in cycles of duration $\Delta t > 0$, the *control period*, each starting at time $t_k = k\Delta t$ $(k = 1, 2, \ldots)$. The computation of the control actions must be amenable to a digital implementation: This is achieved by adopting a *discretize-then-optimize* strategy (Betts, 2010), according to which the predictive model (Section 3.1) and the MPC and MHE optimizations (Sections 3.3 and 3.4) are discretized in time and then solved numerically. Although state-related constraints are commonly *softened* using slack variables (Rawlings et al., 2020), we formulate them as *hard* constraints, as the careful tuning of our controller parameters can guarantee feasibility. The reader is referred to our work (Neto et al., 2024) and to the Supplementary Material for the full details. In the following, we overview the main components of this controller and present their configuration for operating our benchmark WWTP (Section 2.2) for energy-autonomous water resource recovery.

3.1. The predictive model

The predictive controller is based on a representation in state-space form of the wastewater treatment process,

$$\tfrac{d}{dt}x(t) = f(x(t), u(t), w(t) \mid \theta_x); \tag{2a}$$

$$y(t) = g(x(t), u(t) \mid \theta_y); \tag{2b}$$

$$z(t) = h(x(t), u(t) \mid \theta_z). \tag{2c}$$

The state Eq. (2a) models how the N_x state variables evolve given their value $x(t) \in \mathbb{R}^{N_x}$, the value $u(t) \in \mathbb{R}^{N_u}$ of the N_u actionable input (or control variables), and the value $w(t) \in \mathbb{R}^{N_w}$ of the N_w disturbances, at time $t > 0$. The output Eq. (2b) models how the N_y measured outputs $y(t) \in \mathbb{R}^{N_y}$ are formed as emissions of the state $x(t)$ and actions $u(t)$. The performance Eq. (2c) models how the N_z key performance indicators $z(t) \in \mathbb{R}^{N_z}$ are computed from the value of the state $x(t)$ and actions $u(t)$. The vectors θ_x, θ_y, and θ_z collect the constant parameters in the functions f, g, and h, respectively. Since the process has no input feedthrough, we hereafter write $y(t) = g(x(t)|\theta_y)$.

Remark 3. During operation, only the measurement data need to be collected from the instruments in real-time. While the KPIs could be monitored (e.g., to assess the efficacy of the controller), the Output MPC operates by computing these quantities using its predictive model.

The predictive model is assumed to be that provided by the Benchmark Simulation Model no. 2 (Section 2.2)–as such, the controller has knowledge of the *true dynamics* of the system being controlled. While this assumption is rather strict, it enables our proof-of-concept to highlight the capabilities of automatic control of WRRFs without the additional problem of plant-model mismatch. Naturally, the same design can be applied when only a surrogate model of the dynamics is available. Regardless, we remark that the controller has no knowledge of the incoming disturbances and thus its predictions are still imperfect and must rely on accurate estimations of the plant's state from data.

3.2. The operating point optimizer (OPO)

The OPO prepares an operating point that achieves the desired performance while satisfying the constraints. Here, optimality is quantified by the *closeness between the plant's KPIs and some reference profile* set by the plant's management to reflect their economic and environmental targets. An optimal operating point thus consists of state, input, and disturbance vectors at which the plant is in steady-state and its KPIs match the desired profile. The task of computing operating points includes *real-time optimization* (Seborg et al., 2016) and *steady-state target calculation* (Rawlings et al., 2020) approaches, with our formulation inspired by the latter.

For a cycle starting at t_k, the OPO solves the problem

$$\underset{x_k, u_k}{\text{minimize}} \quad \|W_z^{\mathrm{ref}}(z_k - \bar{z}_k^{\mathrm{ref}})\|_2^2 + \|W_u^{\mathrm{ref}}(u_k - \bar{u}_k^{\mathrm{ref}})\|_2^2 \tag{3a}$$

$$\text{subject to} \quad 0 = f(x_k, u_k, \bar{w}_k^{\mathrm{ref}} \mid \theta_x), \tag{3b}$$

$$x_k \in \mathcal{X}^{\mathrm{ref}}, \quad u_k \in \mathcal{U}^{\mathrm{ref}}, \quad z_k \in \mathcal{Z}^{\mathrm{ref}}, \tag{3c}$$

to obtain an operating point $(x_k^{\mathrm{ref}}, u_k^{\mathrm{ref}}) \in \mathbb{R}^{N_x} \times \mathbb{R}^{N_u}$ that produces the optimal KPI values $z_k^{\mathrm{ref}} = h(x_k^{\mathrm{ref}}, u_k^{\mathrm{ref}})$. The vectors $(\bar{z}_k^{\mathrm{ref}}, \bar{u}_k^{\mathrm{ref}}, \bar{w}_k^{\mathrm{ref}})$ are the

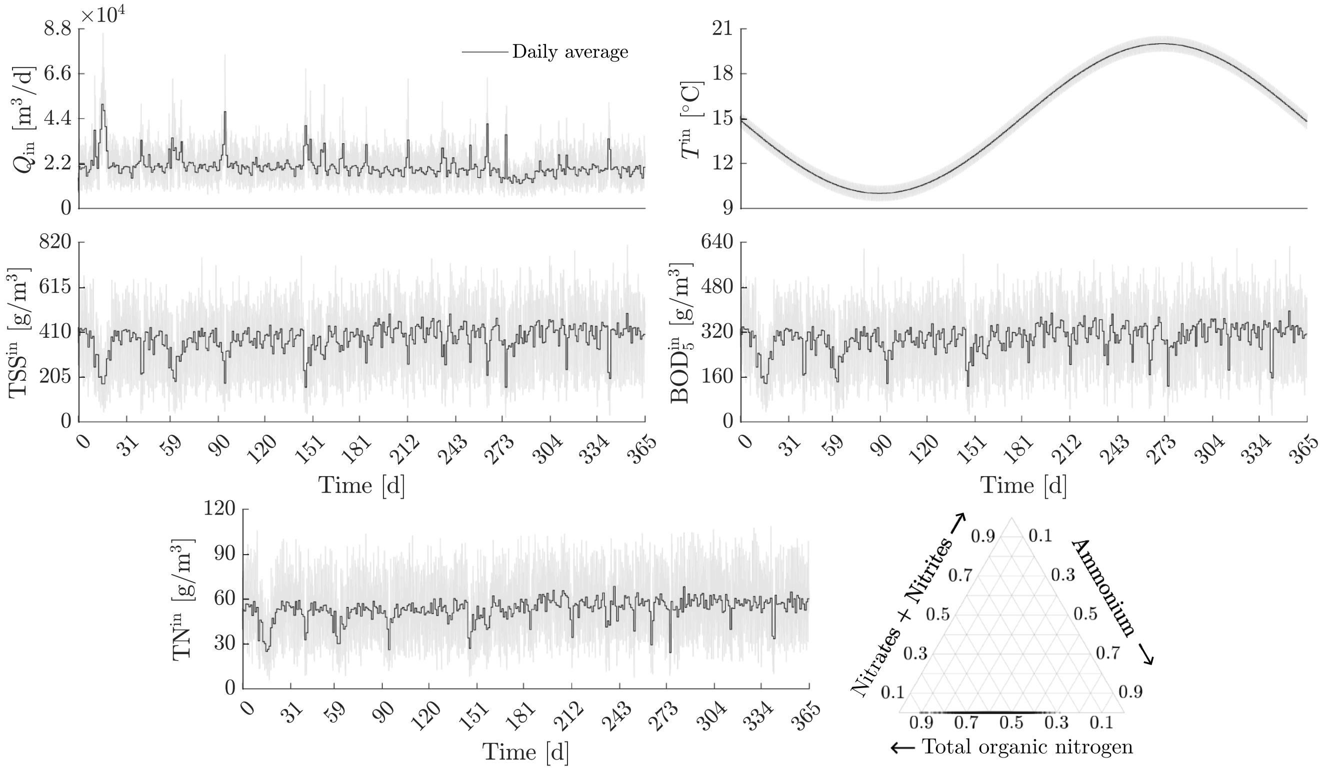

Fig. 3. Wastewater, 1-year period: Influent flow-rate (Q_{in}) and temperature (T^{in}), and its quality in terms of total suspended solids (TSS$^{\text{in}}$), biochemical oxygen demand (BOD$_5^{\text{in}}$) and total nitrogen (TN$^{\text{in}}$). The ternary plot shows the composition of TN$^{\text{in}}$ at each time-step in terms of inorganic (nitrate, nitrite, and ammonium) and total organic nitrogen.

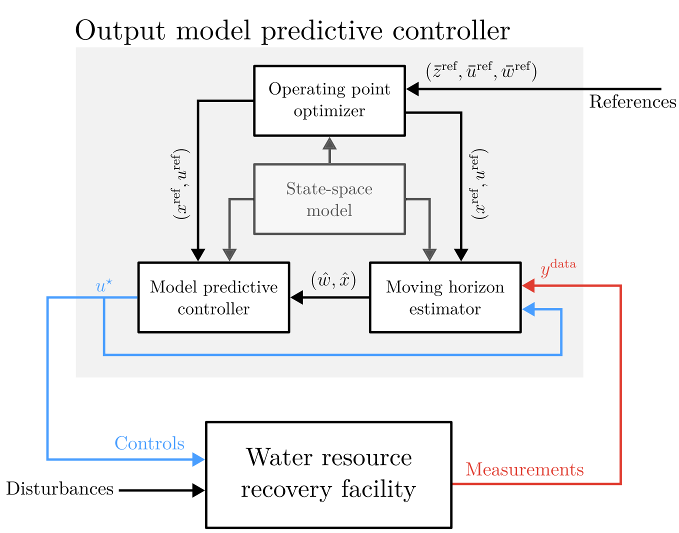

Fig. 4. Main components of the Output MPC.

desired KPIs, actuator configuration, and disturbance profile, respectively, for the kth cycle. The objective function (Eq. (3a)) is defined by the weighting matrices $W_z^{\text{ref}}, W_u^{\text{ref}} \succeq 0$. As customary practice, we consider diagonal matrices (leading to $N_z + N_u$ tuning parameters) with $W_z^{\text{ref}} \succ W_u^{\text{ref}}$ to prioritize matching the desired KPIs rather than the reference actuator setup. The requirement that $(x_k, u_k, \bar{w}_k^{\text{ref}})$ be a steady-state (Eq. (3b)) enables the MPC to stabilize the system around the references (consequently, achieving $\bar{z}_k^{\text{ref}}$). Finally, the constraint sets $\mathcal{X}^{\text{ref}}$, $\mathcal{U}^{\text{ref}}$, and $\mathcal{Z}^{\text{ref}}$, (Eq. (3c)) define which pairs (x_k, u_k) are feasible based on restrictions to be satisfied during the operation of the process. Here, they are taken to describe bound constraints:

$$\mathcal{X}^{\text{ref}} = \{x \in \mathbb{R}^{N_x} \,:\, x_{lb}^{\text{ref}} \preceq x \preceq x_{ub}^{\text{ref}}\}; \tag{4a}$$

$$\mathcal{U}^{\text{ref}} = \{u \in \mathbb{R}^{N_u} \,:\, u_{lb}^{\text{ref}} \preceq u \preceq u_{ub}^{\text{ref}}\}; \tag{4b}$$

$$\mathcal{Z}^{\text{ref}} = \{z \in \mathbb{R}^{N_z} \,:\, z_{lb}^{\text{ref}} \preceq z \preceq z_{ub}^{\text{ref}}\}, \tag{4c}$$

given the collections of lower $\{x_{lb}^{\text{ref}}, u_{lb}^{\text{ref}}, z_{lb}^{\text{ref}}\}$ and upper $\{x_{ub}^{\text{ref}}, u_{ub}^{\text{ref}}, z_{ub}^{\text{ref}}\}$ bounds of appropriate dimensions.

We configure the OPO to implement energy-autonomous resource recovery by having (i) the references $\bar{z}^{\text{ref}}$ enforce a desired water quality, while (ii) the constraints $\mathcal{Z}^{\text{ref}}$ enforce nonpositive energy costs. Specifically, we consider the references $(\bar{z}^{\text{ref}}, \bar{u}^{\text{ref}}, \bar{w}^{\text{ref}})$, bound constraints $(\mathcal{X}^{\text{ref}}, \mathcal{U}^{\text{ref}}, \mathcal{Z}^{\text{ref}})$, and weighting factors $(W_z^{\text{ref}}, W_u^{\text{ref}})$ as in Table 3. This setup is based on extensive experimental campaigns. The weighting for ECI (z_4) removes this variable from the objective function; it is not required to match a specific value, but only to be nonpositive. The desired actuator setup $\bar{u}_k^{\text{ref}}$ and expected disturbances $\bar{w}_k^{\text{ref}}$ are set constant and equal to the values provided by the BSM2: They correspond to the default open-loop controls ($\bar{u}^{\text{ref}}$) when the plant performs nitrogen removal under average influent conditions ($\bar{w}^{\text{ref}}$).

Remark 4. Problem (3) belongs to the class of nonconvex optimization problems and, as such, its solution is computationally demanding. However, the OPO needs to be executed only when changes occur for either the references, the operational constraints, or the expected disturbance profile. As such, its computational burden is not critical.

3.3. *The model predictive controller (MPC)*

The MPC is a state-of-the-art approach to the control of multivariable systems under hard constraints on their state and inputs (Rawlings et al., 2020). This unit computes a sequence of control actions which optimally evolve the system from its current state $x(t_k)$, at time t_k, to the reference state x_k^{ref}, with minimal deviation from the reference input u_k^{ref}.

Table 3
Tuning of the OPO for energy-autonomous resource recovery. The references for the KPIs $z_{1\rightsquigarrow 4}$ depend on the targeted water quality class (A, B, or C). We refer to Table 2 for the units of each variable.

Variable	Reference			Bounds	Weight
	A	B	C		
$\mathrm{TSS}^{\mathrm{eff}}$ (z_1)	10	10	10	$[0,\infty)$	1
$\mathrm{BOD}_5^{\mathrm{eff}}$ (z_2)	4	4	4	$[0,\infty)$	1
$\mathrm{TN}^{\mathrm{eff}}$ (z_3)	7.5	22.5	37.5	$[0,\infty)$	1
ECI (z_4)	0	0	0	$(-\infty,0]$	0
Q_A (u_1)	61944			$[0,92230]$	6e-5
Q_S (u_2)	20648			$[0,36892]$	6e-4
Q_W (u_3)	300			$[0,1844]$	6e-4
Q_R (u_4)	100			$[0,500]$	6e-3
$K_La^{A_1}$ (u_5)	0			$[0,360]$	6e-3
$K_La^{A_2}$ (u_6)	0			$[0,360]$	6e-3
$K_La^{A_3}$ (u_7)	120			$[0,360]$	6e-3
$K_La^{A_4}$ (u_8)	120			$[0,360]$	6e-3
$K_La^{A_5}$ (u_9)	60			$[0,360]$	6e-3
$Q_{\mathrm{EC}}^{A_{1\rightsquigarrow 5}}$ ($u_{10\rightsquigarrow 14}$)	0			$[0,5]$	2e-1
($w_{1\rightsquigarrow 15}$)	See the Supplementary Material				
($x_{1\rightsquigarrow 225}$)	See the Supplementary Material				

The planning is done for a period of time of duration $H_c > 0$, the *control horizon*, under the assumption that (i) the system evolves as the model predicts and that (ii) the disturbances remain constant throughout the control horizon. Accounting for disturbance and model uncertainties, only the first optimal action $u(t_k)$ is deployed to the system then held constant until the next cycle starting at $t_{k+1} = t_k + \Delta t$.

For a cycle starting at t_k, the sequence of optimal actions is the function (of time) $u^\star : [t_k, t_k+H_c] \to \mathbb{R}^{N_u}$ solving

$$\underset{u(\cdot),x(\cdot)}{\text{minimize}} \quad \int_{t_k}^{t_k+H_c} L^c(x(t),u(t))dt + L^f(x(t_k+H_c)) \tag{5a}$$

$$\underset{t\in[t_k,t_k+H_c]}{\text{subject to}} \quad \tfrac{d}{dt}x(t) = f(x(t),u(t),\hat{w}(t_k)), \tag{5b}$$

$$x(t) \in \mathcal{X}^c, \;\; u(t) \in \mathcal{U}^c, \tag{5c}$$

$$x(t_k) = \hat{x}(t_k). \tag{5d}$$

The controller is designed to achieve optimal tracking by minimizing the (squared) distance of the states ($x(t)$) and inputs ($u(t)$) through the control horizon ($t \in [t_k, t_k+H_c]$) to the desired reference (x_k^{ref}, u_k^{ref}) obtained by the OPO. Formally, this is expressed in Eq. (5a) by the cost functions

$$L^c(\cdot,\cdot) = \|W_x\big(x(t) - x_k^{\mathrm{ref}}\big)\|_2^2 + \|W_u\big(u(t) - u_k^{\mathrm{ref}}\big)\|_2^2;$$
$$L^f(\cdot) = \|W_f\big(x(t_k+H_c) - x_k^{\mathrm{ref}}\big)\|_2^2.$$

parametrized by the weighting matrices $W_x, W_f \succeq 0$ and $W_u \succ 0$. We consider diagonal matrices (leading to $N_x + N_u$ tuning parameters) with $W_x \succ W_u$ to prioritize correcting deviations from the reference state. The reader is referred to the Supplementary Material for their explicit values.

The performance of the predictive controller depends on a frequent and consistent deployment of control actions. In its current formulation, however, the problem (5) is nonconvex and thus computationally demanding. We substantially reduce this computational load by converting the dynamic constraints (Eq. (5b)) into linear equalities: Specifically, at the kth cycle, we consider the linearization of the plant's dynamics around the operating point $p_k = (x_k^{\mathrm{ref}}, u_k^{\mathrm{ref}}, \bar{w}_k^{\mathrm{ref}})$,

$$\begin{aligned}\tfrac{d}{dt}x(t) &= f(x(t),u(t),\hat{w}(t_k)) \\ &\approx A_k(x(t)-x_k^{\mathrm{ref}}) + B_k(u(t)-u_k^{\mathrm{ref}}) + G_k(\hat{w}(t_k)-\bar{w}_k^{\mathrm{ref}}),\end{aligned}$$

with $A_k \in \mathbb{R}^{N_x\times N_x}$, $B_k \in \mathbb{R}^{N_x\times N_u}$, and $G_k \in \mathbb{R}^{N_x\times N_w}$ being the first-order variations of $f(\cdot)$ evaluated at p_k,

$$A_k = (\partial f/\partial x)|_{p_k}, \;\; B_k = (\partial f/\partial u)|_{p_k}, \;\; G_k = (\partial f/\partial w)|_{p_k}.$$

This is an accurate approximation of the nonlinear dynamics provided that the controller maintains the plant's state and inputs close to the fixed-point p_k; a valid assumption aside from extreme events. Importantly, the Jacobian matrices (A_k, B_k, G_k) can be computed efficiently and with high accuracy even for large-scale processes (Rawlings et al., 2020).

The design of our MPC is concluded by having the static sets $\mathcal{U}^c$ and $\mathcal{X}^c$ (Eq. 5c) describe bound constraints (that is, minimum and maximum values for the control and state variables). The input signal is enforced to satisfy the actuator limits reported in Table 3 (thus, $\mathcal{U}^c = \mathcal{U}^{\mathrm{ref}}$), while the state signal is only constrained to satisfy volume limits for the reject water tank (thus, $\mathcal{X}^c = \{x : 0 \le x_{211} \le 320\}$).

Finally, we remark that the closed-loop stability of linear-quadratic MPCs depends directly on the constraints $(\mathcal{X}^c, \mathcal{U}^c)$ and terminal weighting matrix W_f (Rawlings et al., 2020, §2.5). Here, W_f is chosen from the solution to the algebraic Riccati equation associated with the unconstrained version of Problem (5). We refer to the Supplementary Material for the full details. Under this setup, our MPC is stabilizing.

3.4. The moving horizon estimator (MHE)

A *dual* to the MPC, the MHE is a state-of-the-art approach to the constrained estimation of (large-scale) systems (Rawlings et al., 2020). This unit is responsible for determining the state $\hat{x}(t_k)$ and disturbance vectors $\hat{w}(t_k)$ used in the MPC (Problem 5): They are the terminal values of the state and disturbance trajectories that solve an optimal state estimation problem, over a past *estimation horizon* of duration H_e. Again, the problem is solved under the assumption that the system evolves as the model predicts. In this case, optimality is defined in terms of *closeness between the past model outputs and plant's measurements* under the controls deployed to the plant over the estimation-horizon.

For a cycle starting at t_k, the state and disturbance estimates are the functions (of time) $\hat{x} : [t_k-H_e, t_k] \to \mathbb{R}^{N_x}$ and $\hat{w} : [t_k-H_e, t_k] \to \mathbb{R}^{N_w}$ solving the problem

$$\underset{w(\cdot),x(\cdot)}{\text{minimize}} \quad L^i(x(t_k-H_e)) + \int_{t_k-H_e}^{t_k} L^e(x(t),w(t))dt \tag{6a}$$

$$\underset{t\in[t_k-H_e,t_k]}{\text{subject to}} \quad \tfrac{d}{dt}x(t) = f(x(t),u^\star(t),w(t)), \tag{6b}$$

$$x(t) \in \mathcal{X}^e, \;\; w(t) \in \mathcal{W}^e. \tag{6c}$$

The estimator is designed to determine the state and disturbance that best explain the plant's data by minimizing the (squared) distance of the model output ($y(t) = g(x(t))$) to the actual measurements ($y^{\mathrm{data}}(t)$) obtained over the past estimation horizon ($t \in [t_k-H_e, t_k]$). This is expressed in Eq. (6a) by the stage and initial cost functions

$$L^e(\cdot,\cdot) = \|W_y\big(y(t) - y^{\mathrm{data}}(t)\big)\|_2^2 + \|W_w\big(w(t) - \bar{w}_k^{\mathrm{ref}}\big)\|_2^2;$$
$$L^i(\cdot) = \|W_i\big(x(t_k-H_e) - \hat{x}_k^{\mathrm{ref}}\big)\|_2^2,$$

parametrized by the weighting matrices $W_y, W_w, W_i \succ 0$. Under this setup, the MHE can be interpreted as a *maximum a posteriori* estimator in which the weighting matrices quantify the uncertainty arising from measurement and process noise (the latter also covering model inaccuracies) (Rao & Rawlings, 2002). We consider diagonal matrices (leading to $N_y + N_w$ parameters) with $W_y \succ W_w$ to prioritize matching the measurement data $y^{\mathrm{data}}(t)$ instead of the expected disturbances $\bar{w}_k^{\mathrm{ref}}$. The reader is referred to the Supplementary Material for the explicit tuning. The initial state reference is defined recursively as $\hat{x}_k^{\mathrm{ref}} = \hat{x}(t_k-H_e+\Delta t)$ with $\hat{x}(\cdot)$ being the estimates from the previous MHE cycle.

The computational load of the estimator is reduced by approximating the plant's model with the linearization,

$$\begin{aligned}\tfrac{d}{dt}x(t) &= f(x(t),u(t),w(t)) \\ &\approx A_k(x(t)-x_k^{\mathrm{ref}}) + B_k(u(t)-u_k^{\mathrm{ref}}) + G_k(w(t)-\bar{w}_k^{\mathrm{ref}}), \\ y(t) &= g(x(t)) \\ &\approx g(x_k^{\mathrm{ref}}) + C_k(x(t)-x_k^{\mathrm{ref}}),\end{aligned}$$

with the same Jacobian matrices (A_k, B_k, G_k) as defined in Section 3.3 and $C_k = (\partial g/\partial x)|_{p_k} \in \mathbb{R}^{N_y \times N_x}$ being the first-order variations of $g(\cdot)$ evaluated at $p_k = (x_k^{\text{ref}}, u_k^{\text{ref}}, \bar{w}_k^{\text{ref}})$.

The design of our MHE is concluded by having the static constraints sets, $\mathcal{W}^e$ and $\mathcal{X}^e$ (Eq. (6c)), to describe bound constraints (that is, minimum and maximum values that disturbance and state variables can take). In our case, the disturbances are known to be nonnegative (thus, we set $\mathcal{W}^e = \mathbb{R}^{N_w}_{\geq 0}$), while the state signal is only constrained by the linearized dynamics ($\mathcal{X}^e = \mathbb{R}^{N_x}$).

Finally, we remark that the convergence of linear-quadratic MHEs depends directly on the constraints ($\mathcal{X}^e, \mathcal{W}^e$) and prior weighting matrix W_i (Rawlings et al., 2020, §4.3). Again, W_i is chosen from the solution to the algebraic Riccati equation associated with the unconstrained version of Problem (6). Under the assumption that the estimation error is bounded, our combined MHE/MPC is then robust asymptotically stable.

4. Simulation results and discussion

This section presents the results obtained by the benchmark WWTP (Section 2.2) when operated by our Output MPC (Section 3) for energy-autonomous resource recovery (Section 2.1). For a realistic simulation, the measurement data (y^{data}) is corrupted with a random process representing real-occurring sensor noise (see the Supplementary Material). We first show how the automatic operation of the plant achieves our primary objective (production of reused water), then we show how it simultaneously achieves our secondary objective (energy-autonomous operation).

4.1. Primary objective: Reused water of tailored quality

The results (Fig. 5) show that the Output MPC can operate the WWTP to provide the requested quality class consistently, despite the influent disturbances. The effluent flow-rate Q_{eff} and temperature T^{eff} are shown to follow closely their influent counterpart: This is expected, as the water line has a constant volume and its reactions are modelled as isothermal. The biochemical profile of the treated water (in terms of TSS^{eff}, $\text{BOD}_5^{\text{eff}}$, and TN^{eff}) shows that the controller can regulate its quality with satisfactory performance except for the sporadic rain and storm events. For the solids and organic matter:

- The effluent total suspended solids (TSS^{eff}) are kept slightly above the 10 g/m^3 reference throughout this 1-year period. The root mean square tracking error is 3.72 g/m^3. Aside from the occasional storm, when TSS^{eff} increases abruptly, we remark on the extreme events occurring at the 1$^{\text{st}}$ month ($t \in [0, 31)$ days) and 10$^{\text{th}}$ month ($t \in [273, 304)$ days). During these events, TSS^{eff} varies notably from the reference and stays uncorrected for a long period. However, the daily-average signal is always below the 30 g/m^3 limit, and thus this KPI complies with the requirements for all quality classes (A, B, and C).
- The effluent 5-days measured biochemical oxygen demand ($\text{BOD}_5^{\text{eff}}$) is kept around the 4 g/m^3 reference throughout this 1-year period. The root mean square tracking error is 1.23 g/m^3. As with TSS^{eff}, the performance is less satisfactory only during extreme events. Because we set a constant $\text{BOD}_5^{\text{eff}}$ reference for all quality classes (see Table 3), the values of this KPI remain consistent throughout the year. Consequently, the daily-average signal is always below the 10 g/m^3 limit, and thus complies with the requirements for all the quality classes (A, B, and C).

The effluent total nitrogen (TN^{eff}), being the nutrient we are interested in recovering, is controlled to change periodically according to the targeted water quality class:

- During odd months, the controller targets quality Class A by regulating TN^{eff} around 7.5 g/m^3. The performance is mostly consistent, with a noticeable but small decline in the 1$^{\text{st}}$ month ($t \in [0, 31)$): In addition to the rain event, the task is more demanding at this period as the lower temperature conditions affect the nitrogen removal efficiency. In contrast, the nitrogen removal efficiency is noticeably higher in the latter months, when temperatures increase. The daily-average signal during odd months is always below the 15 g/m^3 limit, and thus complies with the requirements for reused water of Class A.
- During even months, the controller targets quality Class B by regulating TN^{eff} around 22.5 g/m^3. In this case, performance is less consistent but still satisfactory. The controller struggles to track the reference during the 8$^{\text{th}}$ month ($t \in [212, 243)$) and the 10$^{\text{th}}$ month ($t \in [273, 304)$). Again, this is because higher temperature conditions amplify the nitrogen removal efficiency of this treatment process. Regardless, the daily-average signal during even months is within the $(15, 30]$ g/m^3 limits and thus complies with the requirements for reused water of Class B.
- During the cold season (months 3–5), the controller targets quality Class C by regulating TN^{eff} around 37.5 g/m^3. The reference is tracked consistently, except for a few isolated events. Specifically, the effluent concentrations of this nutrient decrease abruptly at days $t \approx 65$, $t \approx 95$, and $t \approx 145$. These periods align with the occurrence of rain events, indicating that this operational regime is more sensitive to extreme influent disturbances. Regardless, the daily-average signal during this period is mostly within the $(30, 45]$ g/m^3 limits and thus complies with the requirements for reused water of Class C.

The root mean square tracking error for TN^{eff} is 3.17 g/m^3. In Fig. 5, we also visualize the composition of TN^{eff} at each time-step based on the achieved quality class. The results show that the stricter the quality limits, the higher the focus on recovering nitrogen in the form of ammonium. This is not surprising, as the influent nitrogen (Fig. 3) is mostly comprised of organic and ammonium nitrogen: While the former must be removed to avoid violating the quality limits on organic matter (BOD_5), the latter can be recovered by relaxing the nitrogen removal efficiency of the process. The fact that inorganic nitrogen is preferred for crop fertigation, together with the known toxicity of nitrite, makes this chemical profile ideal for clients requesting water of quality Class C (agricultural reuse). Interestingly, this behavior was not explicitly programmed into the controller, but resulted from its planning given the process model and the expected influent profile.

In summary, the results demonstrate the efficacy of this Output MPC strategy and highlight some facts on wastewater treatment and nitrogen recovery. Firstly, it reinforces the well-known fact that nitrogen removal via biological treatment is reduced and amplified, respectively, by low and high temperature conditions. The conjecture is that conventional WWTPs operated as WRRFs should be scheduled to recover nutrients during cold seasons, when producing nitrogen-rich reused water is shown to be a less demanding task. Similarly, the plant can be scheduled to focus on producing cleaner water during warm seasons. Finally, the results show that conventional WWTPs can effectively remove solids and organic matter while simultaneously adjusting the chemical profile of their water effluents.

To understand how the nutrient recovery is achieved, we analyze a selection of the control actions deployed by the Output MPC (Fig. 6). We recall that the controller has been configured to produce control actions that enforce an operation regime with nonpositive energy costs. We focus on the first three months, each corresponding to a distinct quality target, and on the evolution of inorganic nitrogen within the water line. The controller operates this section by manipulating the aeration ($K_L a$) and addition of carbon (Q_{EC}) in all reactors A_r ($r = 1, \ldots, 5$) to optimally adjust the nitrification-denitrification process:

- When targeting Class A (1$^{\text{st}}$ month), the controller increases and decreases, respectively, the aeration to reactors A_2 and A_4 with respect to the nominal values (Table 3). Simultaneously, the controller requests extra carbon to all reactors, with A_4 being supplied the

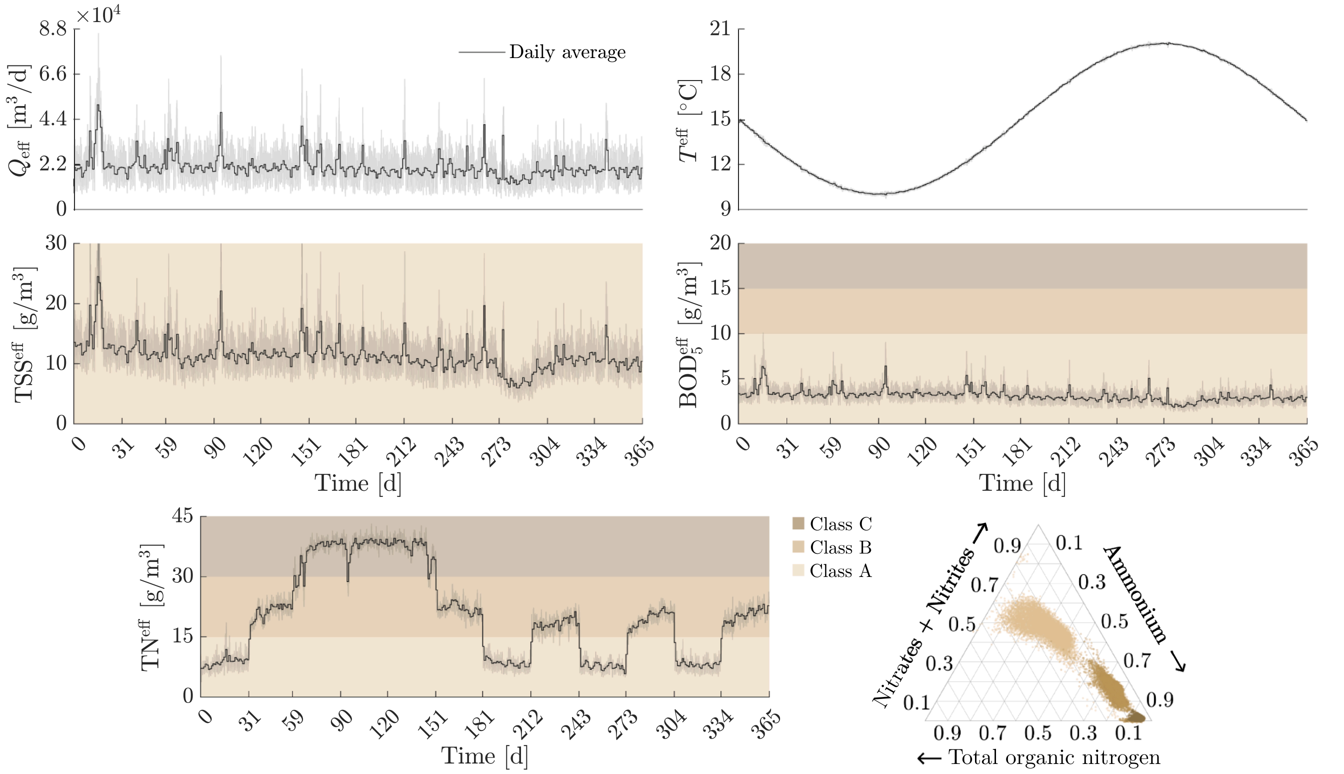

Fig. 5. Simulation, 1-year period: Effluent flow-rate (Q_{eff}) and temperature (T^{eff}), and its quality in terms of total suspended solids (TSS^{eff}), biochemical oxygen demand ($\text{BOD}_5^{\text{eff}}$) and total nitrogen ($\text{TN}^{\text{eff}}$). The shaded regions indicate the different water quality classes (A, B, and C). The ternary plot shows the composition of TN^{eff} at each time-step in terms of inorganic and organic nitrogen forms.

most. Under this configuration, the water line implements a *anoxic-aerated-anoxic-aerated* scheme with denitrification happening in reactors $\{A_1, A_4\}$ and nitrification happening in reactors $\{A_2, A_3, A_5\}$. The state-responses show that nitrate-plus-nitrite nitrogen (S_{NO}) increases while ammonium nitrogen (S_{NH}) is greatly reduced in all reactors, leading to small levels of effluent total nitrogen TN^{eff}.

– When targeting Class B (2nd month), the controller decreases the aeration and slightly increases the carbon addition to all reactors A_r ($r = 1, \ldots, 5$) with respect to the nominal values (Table 3). This leads to the conventional *anoxic-aerated* scheme for activated sludge plants, but with a more conservative aeration profile. The state-responses show that nitrate-plus-nitrite nitrogen (S_{NO}) increases while ammonium (S_{NH}) is only moderately reduced in all reactors, leading to medium levels of effluent total nitrogen TN^{eff}.
– When targeting Class C (3rd month), the controller decreases the aeration to all reactors A_r ($r = 1, \ldots, 5$) with respect to the nominal values (Table 3). As a result, the reactor A_5 is operated under near-anoxic conditions. Simultaneously, the controller requests a small supplement of carbon to all reactors, with emphasis on A_5. This leads to a *anoxic-aerated-anoxic* scheme with only $\{A_3, A_4\}$ being constantly aerated. The state-responses show that nitrate-plus-nitrite nitrogen (S_{NO}) is hardly produced while ammonium (S_{NH}) is kept close to influent levels. Thus, the plant produces high levels of effluent total nitrogen TN^{eff}.

These control actions are strictly inside their feasible sets (see Table 3), with input saturation observed only for the external carbon flow-rates (Q_{EC}) during extreme events.

Adjusting the anoxic/aerated volume of the water line is a well-established strategy for operating biological WWTPs. The Output MPC autonomously finds this strategy and utilizes it to switch between operational modes, while also exploiting the external carbon sources in anoxic zones to compensate for the organic matter consumed in the aerated zones. The degrees-of-freedom enabled by the external carbon sources seemingly led the controller to discover an unconventional treatment scheme (*anoxic-aerated-anoxic-aerated*) for a conventional task (targeting Class A). Formally, the implication is that (according to the predictive model) this is an optimal configuration for efficient nitrogen removal under energy-autonomous restrictions. Finally, we remark on how relaxing the quality limits leads the controller to discover ever-cheaper control strategies– an expected benefit of transitioning WWTPs into WRRFs.

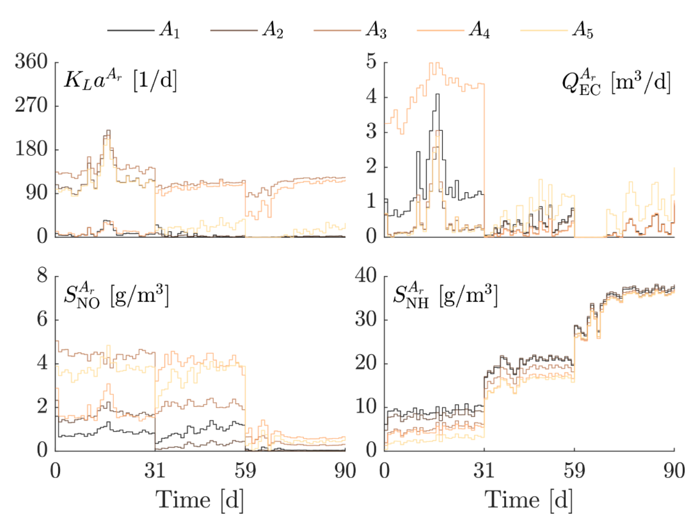

Fig. 6. Simulation, $t \in [0, 90]$: Air ($K_L a$) and external carbon (Q_{EC}) flow-rates, top panels, and nitrate-plus-nitrite (S_{NO}) and ammonium (S_{NH}) nitrogen, bottom panels, for each A_r ($r = 1, \ldots, 5$). Only the daily-average values are displayed.

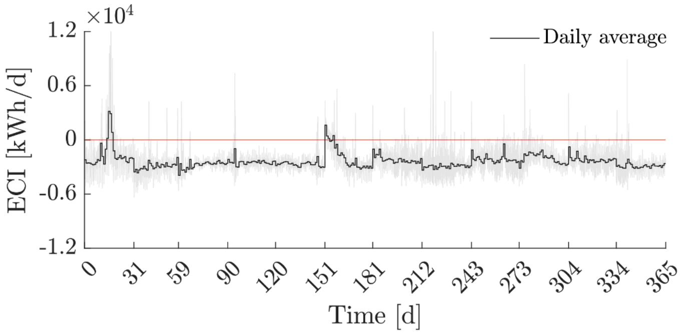

Fig. 7. Simulation, 1-year period: Energy cost index (ECI) during operation. Negative values imply that the process is recovering more heat and electrical energy than needed for driving the plant.

4.2. Secondary objective: Nonpositive energy costs

The results (Fig. 7) show that the operation implemented by the Output MPC is energy-autonomous: Except for two short periods (at days $t \approx 15$ and $t \approx 150$), the energy cost index (ECI) indicates that the plant can recover more heat and electrical energy daily than needed for its operation. The violations of the energy-autonomy constraints align with the occurrence of rain events, highlighting the effect of extreme influent disturbances. For this experiment, the treatment produced a total of 83 GWh, with an average output of 2385 kWh/d of surplus energy. We conjecture that the plant can eliminate the need for buying external electricity (and even benefit from selling its production) by incorporating energy-storage systems into its infrastructure. The achieved energy recovery is also shown to depend on the water quality being targeted:

- When targeting Class A, the output is 2022 kWh/d, on average. On a monthly-basis, this ranges from producing 1607 kWh/d (1$^{\text{st}}$ month, $t \in [0, 31)$ days) to 2178 kWh/d (7$^{\text{th}}$ month, $t \in [181, 212)$ days).
- When targeting Class B, the output is 2534 kWh/d, on average. On a monthly-basis, this ranges from producing 1877 kWh/d (6$^{\text{th}}$ month, $t \in [151, 181)$ days) to 2933 kWh/d (2$^{\text{nd}}$ month, $t \in [31, 59)$ days).
- When targeting Class C, the output is 2635 kWh/d, on average. This production is consistent throughout the cold season, with little variability.

The changes in the energy recovery performance concur with the conclusions from the nutrient recovery task: It is more advantageous to produce water of Class A during warm seasons, whereas producing water of Class B or C benefits from low-temperature conditions. In addition, the results show that set-point changes have a noticeable effect on the ECI. Specifically, switching the reference from Class B to Class A causes a short burst in the energy costs, whereas switching from Class A to Class B causes a sudden decrease. Such an effect is expected considering how quickly the controller changes the aeration regimes when switching the targeted water quality (see Fig. 6).

To understand how the energy recovery is achieved, we again analyze a selection of the control actions deployed by the Output MPC (Fig. 8). We focus on the excess sludge (Q_W) and reject water (Q_R) recycles–the control handles more directly related to the sludge line–, and on the methane production (MP) from the anaerobic digester. Since it comprises most of the costs, we also show the aeration energy (AE) demanded by the water line.

- The results show that the methane production is consistent throughout most of the year, with a noticeable decrease only during the 11$^{\text{th}}$ month. The controller adjusts this production by increasing the wastage flow-rate Q_W when more organic matter needs to be supplied for the anaerobic digester. We remark on the 10$^{\text{th}}$ month ($t \in [273, 304)$ days), when this control handle is saturated while trying to compensate for the decreased influx of organic matter in this period.
- The aeration energy costs are lower the more relaxed the quality limits, as already discussed in Fig. 6. The reject water storage tank, rich in organic matter, is used as a buffer: When energy costs increase (e.g., during set-point changes), the recycle flow-rate Q_R is used to send reject water into the primary clarifier, whose underflow is then sent back to the digester.

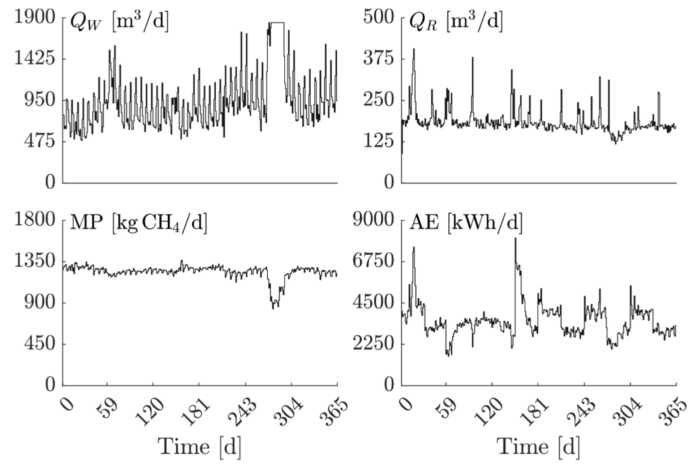

Fig. 8. Simulation, 1-year period: The excess sludge (Q_W) and reject water (Q_R) recycle flow-rates, top panels, and the methane production (MP) and aeration energy (AE), bottom panels. Only the daily-average values are displayed.

While the reject water recycle (Q_R) is always strictly inside its feasible set (see Table 3), note that input saturation occurs for the excess sludge recycle flow-rate (Q_W). Specifically, this control handle saturates when the plant is requested to produce water of Class B under high temperature conditions, evidencing how demanding it is to perform energy-autonomous nutrient recovery in warm seasons.

In summary, the controller enforces an energy-autonomous operation not by boosting biogas production but instead by implementing a regular methane production alongside cheaper aeration schemes. Such a strategy reflects the fact that the controller was explicitly programmed not to minimize energy costs but only to ensure they are nonpositive. Under an alternative tuning, the controller would be able to prioritize energy production, likely at the expense of worsened nutrient recovery. Since our configuration achieves both the primary (resource recovery) and secondary (energy recovery) goals, it contributes a solution to the operation of conventional WWTPs as energy-autonomous WRRFs.

The energy-positive operation of conventional WWTPs implies that such processes can act as *prosumers* (Liu et al., 2022; Zafar et al., 2018). In principle, this (already-existing) infrastructure could be connected to the power grid and, consequently, integrated to the energy market. The plant's management can then choose to buy, sell, or store energy based on its real-time energy demands and on current energy prices. The benefits are bidirectional: The economic costs of operating the plant are alleviated, and the power grid is expanded with a new energy source, strengthening its resilience. The potential to integrate WWTPs into the power grid further illustrates the benefits of transitioning their control objectives from pollution abatement to resource recovery.

5. Concluding remarks

This work presented an automatic control solution for the operation of conventional WWTPs as energy-autonomous WRRFs. We first formalize the task as the production of reused water of different qualities (for either environmental, industrial, or agricultural reuse), while having such an operation result in net-zero energy costs. The effluent water quality is described in terms of its concentrations of total suspended solids (TSS^{eff}), biochemical oxygen demand (BOD_5^{eff}), and total nitrogen (TN^{eff}), and quality classes are defined by upper limits on these metrics. Once the task was formalized, we proposed and configured an output-feedback model predictive controller (Output MPC) comprised of three main computational units: (i) The OPO, which determines an operating point that achieves the desired performance; (ii) the MHE, which estimates the current state of the process based on measurement data; and (iii) the MPC, which computes the control actions that steer the process state to the optimal operating point.

Experimental results demonstrated that such a control strategy is capable of operating a full-scale conventional WWTP as an energy-autonomous WRRF. Specifically, we showed that the controller manipulates the actionable inputs (mainly, the influx of air and supplementary carbon to the water line) to adjust the effluent water quality according to the desired class. The control actions determined by the Output MPC enforce an energy-autonomous operational regime by maintaining a regular production of biogas while decreasing aeration energy costs. The controller performs consistently throughout a year of operation, with a slight decrease in performance observed only during extreme influent events. These results contribute a proof-of-concept on the transitioning of conventional wastewater treatment infrastructure into WRRFs by means of adapting their operation using automation solutions.

In this experimental study, the well-established Benchmark Simulation Model no. 2 (BSM2) is taken as representative of a real-world large-scale treatment plant. This is a pragmatic, but not restrictive, choice. In real-world practice, process engineers would first equip their treatment plants with the necessary actuators/instruments, develop a state-space model of their dynamics, and then follow the steps described here to configure and deploy the controller. While obtaining a first-principles model of such processes might pose a challenge, there exists evidence that black-box models obtained through data-based approaches are sufficiently accurate for control purposes (Bernardelli et al., 2020; Foscoliano et al., 2016; Han et al., 2022). We remark that, under the availability of a predictive model for the process of interest, our control strategy is general enough to accommodate different resource recovery tasks (e.g., phosphorus recovery), influent conditions, and treatment technologies (e.g., membrane bioreactors). In future work, we plan to investigate interconnected treatment-reuse chains in which resource demands arise from the real-time operation of higher-level systems (e.g., crop irrigation systems). Finally, we also plan to expand our control strategy to cover multi-objective tasks (e.g., simultaneously maximizing nutrient and energy recovery) and to achieve offset-free performance by incorporating predictive models for the disturbances.

CRediT authorship contribution statement

Otacílio B. L. Neto: Writing – original draft, Visualization, Software, Methodology, Investigation, Formal analysis, Conceptualization; **Michela Mulas:** Writing – review & editing, Supervision, Conceptualization; **Iiro Harjunkoski:** Writing – review & editing, Supervision; **Francesco Corona:** Writing – review & editing, Writing – original draft, Supervision, Methodology, Conceptualization.

Declaration of competing interest

The authors declare that they have no known competing financial interests or personal relationships that could have appeared to influence the work reported in this paper.

Supplementary material

Supplementary material associated with this article can be found in the online version at 10.1016/j.conengprac.2026.106888.

References

Albornoz, F. (2016). Crop responses to nitrogen overfertilization: A review. *Scientia Horticulturae*, *205*, 79–83. https://doi.org/10.1016/j.scienta.2016.04.026

Alcalde-Sanz, B.M.G.L. (2017). Minimum quality requirements for water reuse in agricultural irrigation and aquifer recharge - towards a water reuse regulatory instrument at EU level, Tech. rep., EUR 28962 EN. Publ. Office of the EU.

Åmand, L., Olsson, G., & Carlsson, B. (2013). Aeration control - a review. *Water Science and Technology*, *67*(1), 2374–2398. https://doi.org/10.2166/wst.2013.139

Batstone, D., Keller, J., Angelidaki, I., Kalyuzhnyi, S., Pavlostathis, S., Rozzi, A., Sanders, W., Siegrist, H., & Vavilin, V. (2002). The IWA Anaerobic Digestion Model No (ADM1), *Water Science and Technology 45*, 65–73. https://doi.org/10.2166/wst.2002.0292

Bernardelli, A., Marsili-Libelli, S., Manzini, A., Stancari, S., Tardini, G., Montanari, D., Anceschi, G., Gelli, P., & Venier, S. (2020). Real-time model predictive control of a wastewater treatment plant based on machine learning. *Water Science and Technology*, *81*(11), 2391–2400. https://doi.org/10.2166/wst.2020.298

Betts, J. T. (2010). Practical methods for optimal control and estimation using nonlinear programming. SIAM.

Brdys, M. A., Grochowski, M., Gminski, T., Konarczak, K., & Drewa, M. (2008). Hierarchical predictive control of integrated wastewater treatment systems. *Control Engineering Practice*, *16*(6), 751–767. https://doi.org/10.1016/j.conengprac.2007.01.008

Busch, J., Elixmann, D., Kühl, P., Gerkens, C., Schlöder, J. P., Bock, H. G., & Marquardt, W. (2013). State estimation for large-scale wastewater treatment plants. *Water Research*, *47*(13), 4774–4787. https://doi.org/10.1016/j.watres.2013.04.007

Chen, R., & Wang, X. C. (2009). Cost-benefit evaluation of a decentralized water system for wastewater reuse and environmental protection. *Water Science and Technology*, *59*(8), 1515–1522. https://doi.org/10.2166/wst.2009.156

Council of the European Union. Regulation (EU) 2020/741 of the European Parliament and of the Council, (2020). https://eur-lex.europa.eu/legal-content/EN/TXT/PDF/?uri=CELEX:32020R0741&from=EN

EPA, U. S. (2012). Guidelines for water reuse.

Faragò, M., Damgaard, A., Madsen, J. A., Andersen, J. K., Thornberg, D., Andersen, M. H., & Rygaard, M. (2021). From wastewater treatment to water resource recovery: environmental and economic impacts of full-scale implementation. *Water Research*, *204*, 117554. https://doi.org/10.1016/j.watres.2021.117554

Foscoliano, C., Del, S., Vigo, M., Mulas, S., & Tronci (2016). Predictive control of an activated sludge process for long term operation. *Chemical Engineering Journal*, *304*, 1031–1044. https://doi.org/10.1016/j.cej.2016.07.018

Francisco, M., Skogestad, S., & Vega, P. (2015). Model predictive control for the self-optimized operation in wastewater treatment plants: Analysis of dynamic issues. *Computers & Chemical Engineering*, *82*, 259–272. https://doi.org/10.1016/j.compchemeng.2015.07.003

Guest, J. S., Skerlos, S. J., Barnard, J. L., Beck, M. B., Daigger, G. T., Hilger, H., Jackson, S. J., Karvazy, K., Kelly, L., Macpherson, L., Mihelcic, J. R., Pramanik, A., Raskin, L., Loosdrecht, M. C. M. V., Yeh, D., & Love, N. G. (2009). A new planning and design paradigm to achieve sustainable resource recovery from wastewater. *Environ. Sci. Technol*, *43*(16), 6126–6130. https://doi.org/10.1021/es9010515

Gernaey, K., Jeppsson, U., Vanrolleghem, P., & Copp, J. (2014). Benchmarking of Control Strategies for Wastewater Treatment Plants (vol. 23). IWA Publ.

Gernaey, K. V., Flores-Alsina, X., Rosen, C., Benedetti, L., & Jeppsson, U. (2011). Dynamic influent pollutant disturbance scenario generation using a phenomenological modelling approach. *Environmental Modelling & Software*, *26*(11), 1255–1267. https://doi.org/10.1016/j.envsoft.2011.06.001

Henze, M., van Loosdrecht, M. C., Ekama, G. A., & Brdjanovic, D. (2008). Biological wastewater treatment. IWA publishing.

Han, H.-G., Chen, C., Sun, H.-Y., & Qiao, J.-F. (2022). Multi-objective integrated optimal control for a wastewater treatment process. *Control Engineering Practice*, *128*, 105296. https://doi.org/10.1016/j.conengprac.2022.105296

Han, H.-G., Qian, H.-H., & Qiao, J.-F. (2014). Nonlinear multiobjective model-predictive control scheme for wastewater treatment process. *Journal of Process Control*, *24*(3), 47–59. https://doi.org/10.1016/j.jprocont.2013.12.010

Han, H.-G., Qiao, J.-F., & Chen, Q.-L. (2012). Model predictive control of dissolved oxygen concentration based on a self-organizing rbf neural network. *Control Engineering Practice*, *20*(4), 465–476. https://doi.org/10.1016/j.conengprac.2012.01.001

Han, M., Yao, J., A, W., Law, K., & Yin, X. (2024). Efficient economic model predictive control of water treatment process with learning-based koopman operator. *Control Engineering Practice*, *149*, 105975. https://doi.org/10.1016/j.conengprac.2024.105975

Henze, M., Gujer, W., Mino, T., & Loosdrecht, M. C. M. V. (2000). Activated sludge models ASM1, ASM2, ASM2D and ASM3. In *Scientific and Technical Report Series No. 9* IWA Publ.

Holenda, B., Dokomosa, E., Rèdey, A., & Fazakas, J. (2008). Dissolved oxygen control of the activated sludge wastewater treatment process using model predictive control. *Computers & Chemical Engineering*, *33*(6), 1270–1278. https://doi.org/10.1016/j.compchemeng.2007.06.008

Kundu, S., Pramanik, B. K., Halder, P., Patel, S., Ramezani, M., Khairul, M., Marzbali, M. H., Paz-Ferreiro, J., Crosher, S., Short, G., Surapaneni, A., Bergmann, D., & Shah, K. (2022). Source and central level recovery of nutrients from urine and wastewater: A state-of-art on nutrients mapping and potential technological solutions. *Journal of Environmental Chemical Engineering*, *10*(2), 107146. https://doi.org/10.1016/j.jece.2022.107146

Kehrein, P., Loosdrecht, M. V., Osseweijer, P., Garfí, M., Dewulf, J., & Posada, J. (2020). A critical review of resource recovery from municipal wastewater treatment plants - market supply potentials, technologies and bottlenecks. *Environmental Science: Water Research & Technology*, *6*, 877–910. https://doi.org/10.1039/C9EW00905A

Li, K., Liu, Q., Fang, F., Luo, R., Lu, Q., Zhou, W., Huo, S., Cheng, P., Liu, J., Addy, M., Chen, P., Chen, D., & Ruan, R. (2019). Microalgae-based wastewater treatment for nutrients recovery: A review. *Bioresource Technology*, *291*, 121934. https://doi.org/10.1016/j.biortech.2019.121934

Liu, Q., Li, R., Dereli, R. K., Flynn, D., & Casey, E. (2022). Water resource recovery facilities as potential energy generation units and their dynamic economic dispatch. *Applied Energy*, *318*, 119199. https://doi.org/10.1016/j.apenergy.2022.119199

Mulas, M., Tronci, S., Corona, F., Haimi, H., Lindell, P., Heinonen, M., Vahala, R., & Baratti, R. (2015). Predictive control of an activated sludge process: An application to the viikinmäki wastewater treatment plant. *Journal of Process Control*, *35*, 89–100. https://doi.org/10.1016/j.jprocont.2015.08.005

Neto, O. B. L., Mulas, M., & Corona, F. (2024). A model-based framework for controlling activated sludge plants. *Chemical Engineering Journal*, *488*, 150750. https://doi.org/10.1016/j.cej.2024.150750

O'brien, M., Mack, J., Lennox, B., Lovett, D., & Wall, A. (2011). Model predictive control of an activated sludge process: A case study. *Control Engineering Practice*, *19*(1), 54–61. https://doi.org/10.1016/j.conengprac.2010.09.001

Olsson, G., Carlsson, B., Comas, J., Copp, J., Gernaey, K., Ingildsen, P., Jeppsson, U., Kim, C., Rieger, L., Rodrìguez-Roda, I., Steyer, J., Takács, I., Vanrolleghem, P., Vargas, A., Yuan, Z., & mand, L. A. (2013). Instrumentation, control and automation in wastewater - from London 1973 to narbonne. *Water Science and Technology*, *69*(7), 1372–1385. https://doi.org/10.2166/wst.2014.057

Olsson, G., Nielsen, M., Yuan, Z., Lynggaard-Jensen, A., & Steyer, J.-P. (2005). Instrumentation, control and automation in wastewater systems. IWA Publ.

Otterpohl, R. (1995). Dynamische Simulation zur Unterstützung der Planung und des Betriebes von kommunalen Kläranlagen. Germany. Technical university of aachen.

Peng, L., Dai, H., Wu, Y., Peng, Y., & Lu, X. (2018). A comprehensive review of phosphorus recovery from wastewater by crystallization processes. *Chemosphere*, *197*, 768–781. https://doi.org/10.1016/j.chemosphere.2018.01.098

Rao, C. V., & Rawlings, J. B. (2002). Constrained process monitoring: Moving-horizon approach. *AIChE Journal*, *48*(1), 97–109. https://doi.org/10.1002/aic.690480111

Rawlings, J. B., Mayne, D. Q., & Diehl, M. M. (2020). Model Predictive Control: Theory, Computation and Design. (2nd ed.). Nob Hill Publ., LLC.

Ricart, S., & Rico, A. M. (2019). Assessing technical and social driving factors of water reuse in agriculture: A review on risks, regulation and the yuck factor. *Agricultural Water Management*, *217*, 426–439. https://doi.org/10.1016/j.agwat.2019.03.017

Sarpong, G., & Gude, V. G. (2020). Near future energy self-sufficient wastewater treatment schemes. *International Journal of Environmental Research*, *14*, 479–488. https://doi.org/10.1007/s41742-020-00262-5

Solon, K., Jia, M., & Volcke, E. I. P. (2019). Process schemes for future energy-positive water resource recovery facilities. *Water Science and Technology*, *79*(9), 1808–1820. https://doi.org/10.2166/wst.2019.183

Santín, I., Pedret, C., Vilanova, R., & Meneses, M. (2016). Advanced decision control system for effluent violations removal in wastewater treatment plants. *Control Engineering Practice*, *49*, 60–75. https://doi.org/10.1016/j.conengprac.2016.01.005

Seborg, D. E., Edgar, T. F., Mellichamp, D. A., & Doyle III, F. J. (2016). Process Dynamics and Control, 4th Edition. John Wiley & Sons.

Shen, W., Chen, X., & Corriou, J. (2008). Application of model predictive control to the BSM1 benchmark of wastewater treatment process. *Computers & Chemical Engineering*, *22*(12), 2849–2856. https://doi.org/10.1016/j.compchemeng.2008.01.009

Shoushtarian, F., & Negahban-Azar, M. (2020). Worldwide regulations and guidelines for agricultural water reuse: A critical review. *Water*, *12*(4), 971. https://doi.org/10.3390/w12040971

Stentoft, P. A., Vezzaro, L., Mikkelsen, P. S., Grum, M., Munk-Nielsen, T., Tychsen, P., Madsen, H., & Halvgaard, R. (2020). Integrated model predictive control of water resource recovery facilities and sewer systems in a smart grid: Example of full-scale implementation in kolding. *Water Science and Technology*, *81*(8), 1766–1777. https://doi.org/10.2166/wst.2020.266

Takács, I., Patry, G., & Nolasco, D. (1991). A dynamic model of the clarification-thickening process. *Water Research*, *25*(10), 1263–1271. https://doi.org/10.1016/0043-1354(91)90066-Y

Valverde-Pérez, B., Ramin, E., Smets, B. F., & Plósz, B. G. (2015). Ebp2r - an innovative enhanced biological nutrient recovery activated sludge system to produce growth medium for green microalgae cultivation. *Water Research*, *68*, 821–830. https://doi.org/10.1016/j.watres.2014.09.027

Verstraete, W., & Vlaeminck, S. E. (2011). Zerowastewater: Short-cycling of wastewater resources for sustainable cities of the future. *International Journal of Sustainable Development & World Ecology* , *18*(3), 253–264. https://doi.org/10.1080/13504509.2011.570804

Vega, P., Revollar, S., Francisco, M., & Martín, J. M. (2014). Integration of set point optimization techniques into nonlinear mpc for improving the operation of wwtps. *Computers & Chemical Engineering*, *68*, 78–95. https://doi.org/10.1016/j.compchemeng.2014.03.027

Wastewater: The untapped resource. (2017). UNESCO. United Nations World Water Assessment Programme.

Wu, B. (2019). Membrane-based technology in greywater reclamation: A review. *Science of The Total Environment*, *656*, 184–200. https://doi.org/10.1016/j.scitotenv.2018.11.347

Wan, J., Gu, J., Zhao, Q., & Liu, Y. (2016). Cod capture: A feasible option towards energy self-sufficient domestic wastewater treatment. *Scientific Reports*, *6*(1), 25054. https://doi.org/10.1038/srep25054

Wang, G., Bi, J., Jia, Q.-S., Qiao, J., & Wang, L. (2023). Event-driven model predictive control with deep learning for wastewater treatment process. *IEEE Transactions on Industrial Informatics*, *19*(5), 6398–6407. https://doi.org/10.1109/TII.2022.3177457

Xie, M., Shon, H. K., Gray, S. R., & Elimelech, M. (2016). Membrane-based processes for wastewater nutrient recovery: Technology, challenges, and future direction. *Water Research*, *89*, 210–221. https://doi.org/10.1016/j.watres.2015.11.045

Yin, X., Decardi-Nelson, B., & Liu, J. (2018). Subsystem decomposition and distributed moving horizon estimation of wastewater treatment plants. *Chemical Engineering Research and Design*, *134*, 405–419. https://doi.org/10.1016/j.cherd.2018.04.032

Yin, X., & Liu, J. (2019). Subsystem decomposition of process networks for simultaneous distributed state estimation and control. *AIChE Journal. American Institute of Chemical Engineers*, *65*(3), 904–914. https://doi.org/10.1002/aic.16426

Zafar, R., Mahmood, A., Razzaq, S., Ali, W., Naeem, U., & Shehzad, K. (2018). Prosumer based energy management and sharing in smart grid. *Renewable and Sustainable Energy Reviews*, *82*, 1675–1684. https://doi.org/10.1016/j.rser.2017.07.018

Zeng, J., & Liu, J. (2015). Economic model predictive control of wastewater treatment processes. *Industrial & Engineering Chemistry Research*, *54*(21), 5710–5721. https://doi.org/10.1021/ie504995n

Zhang, A., Yin, X., Liu, S., Zeng, J., & Liu, J. (2019). Distributed economic model predictive control of wastewater treatment plants. *Chemical Engineering Research and Design*, *141*, 144–155. https://doi.org/10.1016/j.cherd.2018.10.039